

Training with Product Digital Twins for AutoRetail Checkout

Yue Yao^{1*†}, Xinyu Tian^{1*}, Zheng Tang², Sujit Biswas², Huan Lei³, Tom Gedeon⁴, Liang Zheng¹

¹The Australian National University

²NVIDIA

³The University of Adelaide

⁴Curtin University

Abstract

Automating the checkout process is important in smart retail, where users effortlessly pass products by hand through a camera, triggering automatic product detection, tracking, and counting. In this emerging area, due to the lack of annotated training data, we introduce a dataset comprised of product 3D models, which allows for fast, flexible, and large-scale training data generation through graphic engine rendering. Within this context, we discern an intriguing facet, because of the user “hands-on” approach, bias in user behavior leads to distinct patterns in the real checkout process. The existence of such patterns would compromise training effectiveness if training data fail to reflect the same. To address this user bias problem, we propose a training data optimization framework, *i.e.*, training with digital twins (DtTrain). Specifically, we leverage the product 3D models and optimize their rendering viewpoint and illumination to generate “digital twins” that visually resemble representative user images. These digital twins, inherit product labels and, when augmented, form the Digital Twin training set (DT set). Because the digital twins individually mimic user bias, the resulting DT training set better reflects the characteristics of the target scenario and allows us to train more effective product detection and tracking models¹. In our experiment, we show that DT set outperforms training sets created by existing dataset synthesis methods in terms of counting accuracy. Moreover, by combining DT set with pseudo-labeled real checkout data, further improvement is observed. The code is available at <https://github.com/yorkeyao/Automated-Retail-Checkout>.

Introduction

In the rapidly evolving landscape of smart retail, the automation of processes has emerged as a pivotal endeavor, enhancing efficiency and user experience. One prominent facet of this transformation is the automation of the checkout process, wherein users seamlessly pass products through a camera-enabled environment, eliciting automated product detection, tracking, and counting. This innovative paradigm streamlines the shopping experience but also

*These authors contributed equally.

†This work is partially done when Yue has an internship at NVIDIA.

¹Counting is an inherent outcome once all products are successfully detected and tracked.

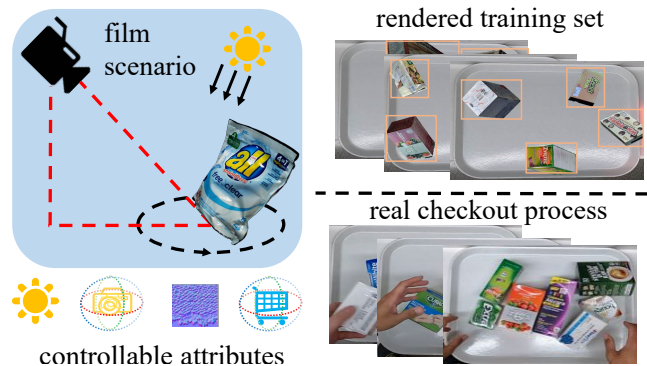


Figure 1: Problem definition. We focus on the problem of using 3D assets for training 2D detection and tracking model for AutoRetail Checkout. Given 3D assets, we aim to render a 2D training set by setting up a filming scenario. To achieve this, we propose a DtTrain framework, to improve the training set specificity on the real checkout process.

presents unique challenges, particularly in the realm of data acquisition and model training.

To achieve AutoRetail Checkout (ARC) with deep learning, the acquisition of labeled training data has become a significant bottleneck, due to its difficulty in data collection, expensive annotation, and privacy concerns (Ristani et al. 2016). For example, collecting real AutoRetail Checkout training data could be costly, as it typically involves manual product movement in front of a camera and subsequent time-consuming human labeling. In this paper, we avoid the usage of real data labeling and introduce a novel dataset that leverages product 3D models as a foundation for training data generation. Shown in Fig. 1, given 3D product models, employing a renderer allows rapid generation of rendered product images, producing a training set with thousands of images within minutes. (Richter et al. 2016; Sakaridis, Dai, and Van Gool 2018; Ruiz, Schuster, and Chandraker 2019; Tremblay et al. 2018; Sun and Zheng 2019).

Though data rendering using graphic engines offers significant advantages for training deep learning models, it introduces a distinctive challenge, *i.e.*, the bias difference (termed as domain gap) between rendered and real data, which hampers its scalability. To explain, as users interact with the ARC in a “hands-on” manner, these individual bi-



Figure 2: 3D assets and real image examples in automatic retail checkout dataset. We have 3D assets for model training and 2D images for model validation and testing.

ases manifest as discernible patterns in the resulting product images. For instance, many customers tend to place the labeled side of the product facing upwards, resulting in the camera being more likely to capture this biased viewpoint. In this case, if the training data fails to encapsulate these biases, the presence of such a domain gap introduces a hurdle to the efficacy of training, as models may not generalize effectively to real-world scenarios.

In the past, addressing domain gap and making rendered data more realistic required extensive human effort, involving complex filming scene arrangements. However, recent advancements in computer vision have brought about a revolutionary change in film scene arrangement techniques. These advancements enable training set optimization and reduce the necessity for extensive human involvement in the process (Kar et al. 2019; Ruiz, Schuler, and Chandraker 2019; Yao et al. 2020, 2022). A prime example of these advancements is the attribute descent algorithm developed by Yao *et al.* This algorithm efficiently learns film attribute distributions, significantly enhancing the realism of rendered data and improving the specificity of the training set for a target validation/testing (Yao et al. 2020, 2022). With these methods, the gap between rendered and real data is narrowed, making rendered datasets more valuable for training deep learning models.

In this paper, we present a novel pipeline for rendered training set creation by augmenting core digital twins. Firstly, our approach is motivated by the understanding that the target set bias can be effectively represented by its smaller core set. To create this core set, we carefully select the most representative samples from the target domain based on their similarity in the feature space. For representative images, we utilize the graphic engine to create their digital twins, which are virtual representations of products in the rendering environment that closely mimic real images. This is achieved through precise per-image attribute optimization with coordinate descent (Wright 2015). Subsequently, we apply attribute-guided data augmentation techniques to these digital twins, thereby substantially increasing the dataset size. This data generation process culminates in the formation of the Digital Twin training set (DT set), a training dataset that specifically encapsulates the "hands-on" user bias.

We conduct a comprehensive experiment to illustrate the superior efficacy of the DtTrain over existing training set creation methods in terms of ARC counting accuracy. Furthermore, when having joint training of the DT set and pseudo-labeled real checkout data, it results in demonstra-

Datasets		#Cate.	#Images	Modality	Attr
Multi-modal Retrieval	Dress Retrieval	50	0.020M	I,T	✗
	Product1M	458	1.182M	I,T	✗
	MEP-3M	599	3.012M	I,T	✗
	M5Product	6,232	6.313M	I,T,V,A,Tab	✗
Retail Checkout	RPC	200	0.368M	I	✗
	ARC (Ours)	116	∞	V	✓

Table 1: Comparing datasets related to retail objects. "Attr" denotes whether the dataset has attribute labels (*e.g.*, orientation). In our ARC dataset, a category is a 3D model corresponding to a product. From each 3D model (category), we can render an unlimited number of images by varying environment and camera settings in Unity. Modalities are denoted as: Image (I), Text (T), Video (V), Audio (A), and Table (Tab).

ble performance enhancements. Through this endeavor, the study offers a promising solution to the conundrum of user bias, ultimately advancing the frontier of automated checkout systems in smart retail.

Method

Automatic Retail Checkout Dataset

In this paper, the challenge lies in the absence of a labeled real-world training set for ARC. We address this by rendering different images from the given 3D retail models. The rendered data allows us to train a robust model for the 2D ARC task, even in an environment with no prior annotations for the validation/test set.

To accomplish this task, we introduce a novel dataset specifically designed for ARC. Fig. 1, Fig. 2 and Table 1 illustrate examples and statistics of this dataset. We have curated 116 3D scans of real-world retail objects sourced from supermarkets, represented as 3D models. The dataset encompasses various object classes, including daily necessities, food, toys, furniture, and household items, among others. The images are captured in a setup from Yao et al. (2022). As depicted in Fig. 1 left, we incorporate controllable attributes like object placement, camera pose, and lighting. As highlighted in Table 1, compared to Dress Retrieval (Corbiere et al. 2017), Product1M (Zhan et al. 2021), MEP-3M (Liu et al. 2023), M5Product (Dong et al. 2022), and RPC (Wei et al. 2019), our dataset stands out by providing 3D assets, which offer the potential to generate an extensive collection of images. Additionally, the rendered data enables us to provide accurate product labeling and further attribute labeling for real checkout scenarios. To promote collaboration and further research, we will make the 3D models and film scene (implemented by a Unity-Python interface) readily available to the community, allowing the creation of more rendered data if required.

In a real ARC scenario, shown in the bottom right corner of Fig. 1, the camera is mounted above the checkout counter and facing straight down, while a customer is enacting a checkout action by "scanning" objects in front of the counter in a natural manner. Several different customers participate, and each of them scan slightly differently. There is a shopping tray placed under the camera to indicate where

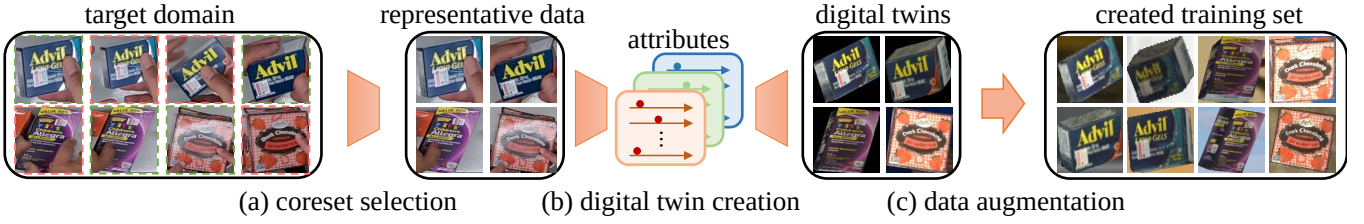


Figure 3: The DtTrain framework. It is designed to construct bias-adapted rendered training data. The framework comprises three key components: (a) coreset selection, aiming at identifying the most representative samples from the target domain. In the figure, the target images with green dashed boxes are selected, and those with red dashed boxes are not selected. Following this, we (b) generate digital twins for each image within the core set, by optimizing attributes shown in Fig. 1. Ultimately, the training set is curated through (c) attribute-guided data augmentation based on the rendered core set.

the AI model should focus. In summary, we obtain approximately 22 minutes of videos, and the videos are further split into target unlabeled *training* and labeled *test* sets such that *training* and *test* account for 40% and 60%, respectively.

The presence of a noticeable domain gap between the rendered source and real target data is our major concern. Real-world datasets often exhibit distinct dataset biases, *e.g.*, viewpoint bias. During a retail checkout process, customers typically view products from specific angles, resulting in uneven distribution of viewpoints. For instance, plate-like products are usually viewed from the front or rear as people handle them manually. If our rendered training set lacks a similar bias in viewpoint distribution, it creates a discrepancy between the two domains. As a consequence, the model’s performance may suffer such a domain gap, leading to a drop in accuracy and effectiveness.

Problem Definition

Formally, we denote the *target* real ARC dataset as $\mathcal{D}_T = \{(\mathbf{x}_i, y_i)\}_{i=1}^M$ where M indicates the number of image-label pairs in the target. It follows the distribution p_T , *i.e.*, $\mathcal{D}_T \sim p_T$. Let \mathcal{D}_S be the rendered *source* set to be constructed, and $\mathcal{D}_S = \{(\mathcal{R}(\psi_i), y_i)\}_{i=1}^N$. Here ψ_i is an attribute vector of K components controlling the 3D rendering environment, *i.e.*, $\psi_i = [\mu_1, \dots, \mu_K] \in \mathbb{R}^K$. $\mathcal{R}(\cdot)$ is the underlying rendering function that takes attribute vector ψ_i as input and produces a rendered image. We input attribute ψ_i to the renderer that generates an image-label pair. With our renderer, we can potentially render an unlimited number of images. But here we have N indicates the desired number of image-label pairs in the rendered dataset.

With these definitions, in this paper, we aim to build \mathcal{D}_S^* with an objective that the model $h_{\mathcal{D}_S}$ trained on \mathcal{D}_S has minimized risk on \mathcal{D}_T , *i.e.*,

$$\mathcal{D}_S^* = \arg \min_{\mathcal{D}_S} \mathbb{E}_{\mathbf{x}, y \sim p_T} [\ell(h_{\mathcal{D}_S}(\mathbf{x}), y)]. \quad (1)$$

In this paper, since we actually do not have labels in \mathcal{D}_T , The optimization objective we define in Eq. 1 is not directly tractable. Thus, we need to build \mathcal{D}_S^* without performing real training and testing. Alternatively, we aim to get \mathcal{D}_S^* which trains a model that can have similar performance as \mathcal{D}_T , which is a real target training set. Thus, formally, we transfer the objective as:

$$\mathcal{D}_S^* = \arg \min_{\mathcal{D}_S} |L(h_{\mathcal{D}_T}(\mathbf{x}), y) - L(h_{\mathcal{D}_S}(\mathbf{x}), y)|, \quad (2)$$

where $L(h_{\mathcal{D}_T}(\mathbf{x}), y)$ and $L(h_{\mathcal{D}_S}(\mathbf{x}), y)$ are the respective risks of model h on the dataset \mathcal{D}_T and \mathcal{D}_S . For explicitly, we define the risk of model h on an arbitrary dataset \mathbf{S} as

$$L(h_{\mathbf{S}}(\mathbf{x}), y) = \frac{1}{|\mathbf{S}|} \sum_{(\mathbf{x}_i, y_i) \in \mathbf{S}} \ell(h_{\mathbf{S}}(\mathbf{x}_i), y_i), \quad (3)$$

where $\ell(h_{\mathbf{S}}(\mathbf{x}_i), y_i)$ is the risk on individual samples as in Eq. 1.

We further split our objective into two parts, where we aim to optimize the upper bound of the error in Eq. 2, *i.e.*,

$$\mathcal{D}_S^* = \arg \min_{\mathcal{D}_S} \underbrace{|L(h_{\mathcal{D}_T}(\mathbf{x}), y) - L(h_{\mathcal{D}_C}(\mathbf{x}), y)|}_{\text{Core Set Error}} + \underbrace{|L(h_{\mathcal{D}_C}(\mathbf{x}), y) - L(h_{\mathcal{D}_S}(\mathbf{x}), y)|}_{\text{Digital Twin Error}}. \quad (4)$$

Coreset Selection

In the first part, to ensure similar performance between the model trained on \mathcal{D}_C and the model trained on \mathcal{D}_T , we minimize the risk differences between them, *i.e.*,

$$\mathcal{D}_C = \arg \min_{\mathcal{D}_C \in 2^{\mathcal{D}_T}} |L(h_{\mathcal{D}_T}(\mathbf{x}), y) - L(h_{\mathcal{D}_C}(\mathbf{x}), y)|, \quad (5)$$

where \mathcal{D}_C is a subset of \mathcal{D}_T in the size O , *i.e.*, $\mathcal{D}_C = \{(\mathbf{x}_i, y_i)\}_{i=1}^O$. Thus, we reduce the problem into a core set selection problem.

From the theory of core set (Sener and Savarese 2018), if \mathcal{D}_C is the δ cover of the set \mathcal{D}_T and shares the same number of classes with \mathcal{D}_T , the risk difference between model $h_{\mathcal{D}_S}$ and $h_{\mathcal{D}_S}$ (*i.e.*, core set error) is bounded by

$$|L(h_{\mathcal{D}_T}(\mathbf{x}), y) - L(h_{\mathcal{D}_C}(\mathbf{x}), y)| \leq O(\delta) + O(|\mathcal{D}_T|^{-\frac{1}{2}}). \quad (6)$$

δ is the radius of the cover, and $O(\delta)$ is a polynomial function over δ . The problem can be reduced as a K-center problem (Farahani and Hekmatfar 2009) by optimizing $O(\delta)$. We apply a 2-approximation algorithm (Williamson and Shmoys 2011) to iteratively find optimal samples in \mathcal{D}_T and add to \mathcal{D}_C . Specifically, each optimal sample \mathbf{z}^* is computed as

$$\mathbf{z}^* = \arg \max_{\mathbf{z}_i \in \mathcal{D}_C \setminus \mathcal{D}_T} \min_{\mathbf{z}_j \in \mathcal{D}_T} \|f(\mathbf{x}_i) - f(\mathbf{x}_j)\|_2, \quad (7)$$

where $\mathbf{z} = (\mathbf{x}, y)$, and $f(\mathbf{x})$ represents the feature extracted of an image \mathbf{x} . This process is named the furthest point sampling (FPS) method (Eldar et al. 1997), which enables the

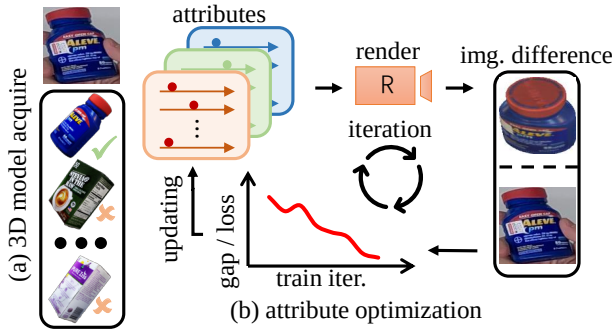


Figure 4: The pipeline to obtain the digital twins. Given a 2D real image, we built its digital twin by firstly (a) acquiring the 3D assets by pseudo labeling. (b) Upon that, we render the selected 3D asset in terms of a vector of attributes, which will be iteratively optimized by coordinate descent using the image-wise difference between the rendered image and the target real image.

most representative samples from a dataset to be selected iteratively until size O .

Digital Twin Creation

We then focus on the second part, we aim to get

$$\mathcal{D}_S^* = \arg \min_{\mathcal{D}_S} |L(h_{\mathcal{D}_C}(\mathbf{x}), y) - L(h_{\mathcal{D}_S}(\mathbf{x}), y)|. \quad (8)$$

as \mathcal{D}_C can be relatively small in scale (since it is a pruned set from \mathcal{D}_T), we consider dataset \mathcal{D}_S^* to be identical to \mathcal{D}_C by forming digital twins, by minimizing the content difference in every single image between them. Formally, we have the rendered dataset $\mathcal{D}_S^* = \{(\mathcal{R}(\psi_i), y_i)\}_{i=1}^O$ and coreset $\mathcal{D}_C = \{(\mathbf{x}_i, y_i)\}_{i=1}^O$. For each sample \mathbf{x}_i in coreset \mathcal{D}_C , we aim to optimize ψ_i , *i.e.*,

$$\psi_i^* = \arg \min_{\psi_i} \|f(\mathbf{x}_i) - f(\mathcal{R}(\psi_i))\|_2, \quad (9)$$

where $f(\cdot)$ denotes the feature extraction function in the feature space. In real practice, we use LPIPS (Zhang et al. 2018) to calculate image differences in feature space.

To optimize ψ_i , we are inspired by attribute descent (Yao et al. 2022) and use an adapted version for obtaining digital twins, *i.e.*, coordinate descent (Wright 2015) for per-image optimization. Specifically, we aim to achieve the goal iteratively. Initially, at epoch j , we have

$$\psi_i^0 = [\mu_1^0, \dots, \mu_K^0]. \quad (10)$$

At epoch j and iteration k , we iteratively optimize a single variable μ_k^j ,

$$\mu_k^j = \arg \min_{z \in S_k} \|f(\mathbf{x}_i) - f(\mathcal{R}(\psi_i^j))\|_2, \quad (11)$$

where

$$\psi_i^j = [\mu_1^j, \dots, \mu_{k-1}^j, z, \mu_{k+1}^{j-1}, \dots, \mu_M^{j-1}], \quad (12)$$

and $S_k, k = 1, \dots, K$ defines the search space for μ_k . For example, the search space for the azimuth is between 0° and 330° by 30° degree intervals.

In this paper, an iteration is defined as the duration for which a single attribute undergoes coordinate descent optimization. An epoch is a duration for which all attributes undergo one attribute descent round. In this algorithm, each iteration performs a greedy search for the optimized value of an attribute while values of the other attributes are fixed. Therefore, each iteration finds the attribute value for a single attribute, and an epoch gives values for the entire attribute vector. In our experiments, the entire optimization process usually converges in 2 epochs.

Attribute-guided Augmentation

From the previous step, we get a set of core digital twins $\mathcal{D}_S^* = \{(\mathcal{R}(\psi_i), y_i)\}_{i=1}^O$. Though it can be used for training models directly, its dataset size O can be small in size as we performed a coreset selection. To increase the dataset size to a desired number N , we perturb the optimized attribute values to introduce the diversity of the training set. We randomly pick an optimized attribute vector ψ_i^* , we apply a multivariate Gaussian perturbation, denoted as $\alpha_j \sim \mathcal{N}(\psi_i^*, \Sigma)$, where Σ is a pre-defined diagonal covariance matrix, and i samples from a uniform distribution from 1 to O , *i.e.*, $i \sim \mathcal{U}(1, O)$. To achieve a varied dataset resembling the digital twins, we need to strike a balance with the variance. Typically, we opt for a variance that keeps most of the values within a 15% deviation from the mean. Given such a process, we apply augmentation multiple times to sample our final training set \mathcal{S} (DT set) until it reaches size N , *i.e.*,

$$\mathcal{S} = \{(\mathcal{R}(\alpha_j), y_j)\}_{j=1}^N, \quad (13)$$

where $\alpha_j \sim \mathcal{N}(\psi_i^*, \Sigma)$, and $i \sim \mathcal{U}(1, O)$.

Experiment

Experiment Details

Task setting. The videos are split such that 40% of the data is to be used for target training. We are tasked to create a rendered training set by adapting to the given unlabeled target training videos, train a model on the rendered data, and report the task test accuracy on the remaining 60% of the data, named as the target test set.

Task model. Once we get the optimized rendered data, we train the ARC model using the detection-tracking-counting framework as depicted from Nguyen, Phan, and Nguyen (2022). The pseudo-labeling model is trained from random attributes. More details are in the supplementary material.

Evaluation metrics. Our model evaluation entails aligning the dual outputs with the ground truth. A prediction is deemed accurate if and only if both the predicted *label* and *its corresponding timeframe* are correct. Specifically, we have precision, signifying the ratio of correct predictions to total predictions, and recall, reflecting the ratio of correct predictions to total ground truth. The culmination of these metrics is represented by an F1 score. Furthermore, we employ the Fréchet Inception Distance (FID) (Heusel et al. 2017) to assess the domain gap between the rendered set generated and the target set.

Methods in comparison. In this study, we conduct a comprehensive comparison between our proposed DfTrain

Type	Method	Bag				Box				Bottle				All			
		FID↓	F1↑	Prec.↑	Recall↑	FID↓	F1↑	Prec.↑	Recall↑	FID↓	F1↑	Prec.↑	Recall↑	FID↓	F1↑	Prec.↑	Recall↑
Random		243.38	11.76	20.00	8.33	220.76	29.12	26.37	32.52	228.14	41.38	49.98	35.29	220.41	27.92	27.98	27.85
Dist. opt.	LTS	214.85	45.78	58.08	37.78	177.36	32.02	29.61	34.85	189.04	34.02	40.10	29.54	179.62	33.46	30.29	37.21
	Attr. Desc.	203.38	57.14	66.67	50.00	152.84	39.66	37.30	42.33	134.31	40.00	34.78	47.06	166.37	40.60	39.13	42.19
Digital Twin	InfoGAN	237.50	50.00	62.50	41.67	187.48	30.08	27.55	33.13	172.10	25.81	28.57	23.53	189.42	30.73	28.90	32.81
	Soft Ras.	211.69	27.27	30.00	25.00	172.13	34.02	32.58	35.58	153.65	43.75	46.67	41.18	171.70	34.43	33.50	35.42
	LDM	186.59	35.29	60.00	25.00	149.46	41.32	39.50	44.01	143.56	37.50	40.00	35.29	147.76	40.78	38.18	43.75
	Coord. Desc	177.64	55.56	83.33	41.67	128.49	42.32	40.11	44.79	122.95	48.48	50.00	47.06	128.11	43.43	42.16	44.79

Table 2: Comparing different training set creation methods. We report ARC counting accuracy and FID for *bag*, *box*, *bottle*, and *all* products in different columns (all metrics are in percentage except FID). We report accuracy when training with rendered data only.

Selection	Bag		Box		Bottle		All	
	FID↓	F1↑	FID↓	F1↑	FID↓	F1↑	FID↓	F1↑
Random	170.99	44.44	133.26	41.55	119.31	47.06	133.04	42.13
FPS	167.64	55.56	128.49	42.32	112.95	48.48	128.11	43.43

Table 3: Comparison of different coreset selection methods. Notations and evaluation metrics are the same as in the previous table.

Loss	Bag		Box		Bottle		All	
	FID↓	F1↑	FID↓	F1↑	FID↓	F1↑	FID↓	F1↑
SSIM	172.30	47.62	134.32	41.00	115.42	51.43	133.51	42.21
StyleLoss	182.24	35.71	123.66	44.44	134.35	30.30	135.23	42.76
LPIPS	167.64	55.56	128.49	43.32	122.95	48.48	128.11	43.43

Table 4: Comparison of different loss functions. Notations and evaluation metrics are the same as in the previous table.

framework and two established methods commonly employed for generating training sets through the graphic engine, namely LTS (Ruiz, Schuler, and Chandraker 2019) and attribute descent (Yao et al. 2022). These methods fall under the category of attribute distribution optimization, as they necessitate the prior definition of attribute distributions and subsequent parameter optimization.

Several existing approaches for acquiring digital twins exist. Within the DtTrain framework, we compare these approaches with the coordinate descent algorithm employed in our research. Specifically, digital twin acquisition can also be achieved through the utilization of the differentiable renderer, known as the soft rasterizer (Liu et al. 2019). Additionally, we incorporate neural rendering techniques to procure digital twins, including InfoGAN (Chen et al. 2016) and latent diffusion models (LDM) (Rombach et al. 2022). For a comprehensive understanding of the comparative methods, we provide intricate details in the supplementary material.

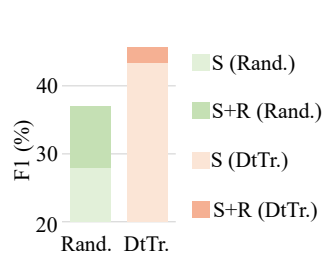


Figure 5: Comparing training sets created by DtTrain and random attributes. Two application scenarios are evaluated: training with rendered data only (“S”) and joint training on both pseudo-labeled real data and rendered data (“R+S”).

Main Results

The superiority of DtTrain over random attributes, and existing dataset synthesis methods. We compare the proposed DtTrain to random attributes under two settings. As shown in Fig. 5, in the first setting, we only use the rendered data to train an ARC model. In the second setting, we use the rendered data combined with the pseudo-label real data to train an ARC model. Under both settings, we observe a notable superiority of DtTrain over random attributes.

Table 2 displays evaluation results for various optimization methods, categorized by two training set creation pipelines. Notably, DtTrain outperforms existing attribute distribution optimization methods. For example, when creating digital twins with coordinate descent, the created training set surpasses the distribution optimization technique attribute descent by 2.6% F1 score.

Our understanding of the difference between attribute distribution optimization and our proposed pipeline aligns with the observed results. Digital twin creation involves image-to-image representations, with each product characterized by multiple augmented attribute vectors for a more intricate distribution. This highlights a key distinction that the assumption in attribute distribution optimization limits simulation potential, while our approach with multiple digital twins fosters a richer distribution. Adopting a more intuitive perspective, this image-to-image alignment eliminates interference from diverse backgrounds in digital twin creation, especially beneficial in object-centric tasks like ARC where unexpected perceptual noise can disrupt results.

Enhanced accuracy through joint training with pseudo-labeled target data. As depicted in Fig. 5, our find-

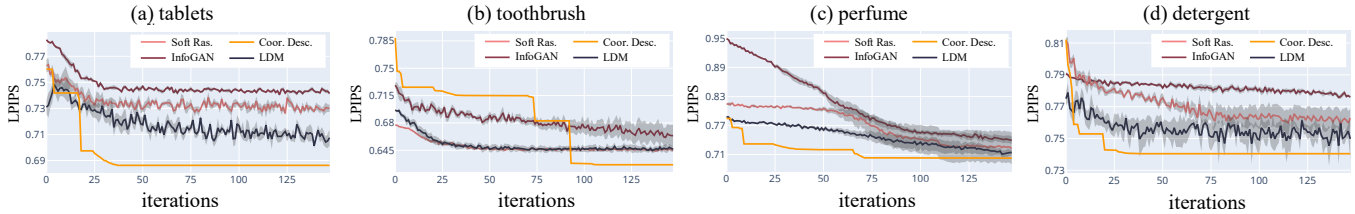


Figure 6: Convergence study of digital twin creation methods. We select 4 sample products randomly from the dataset, which include 2 boxes (tablets and toothbrush), 1 bottle (perfume), and 1 bag (detergent). We plot the loss trend for each product during the optimization process using different methods: soft rasterizer, coordinate descent InfoGAN based and LDM based neural rendering. Among these methods, coordinate descent stands out with its distinct optimization curve, characterized by a step-like descent trend. This unique behavior is attributed to coordinate descent being a search algorithm.

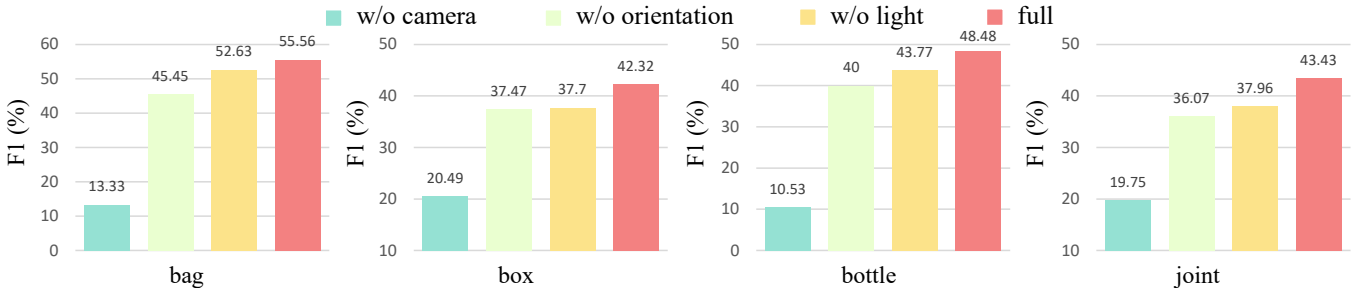


Figure 7: Ablation study on attributes. We divide the attribute vector into camera (height and distance), orientation (azimuth and in-plane rotation), and light (intensity). By separately analyzing the role of each attribute group in optimization and comparing it to the full optimization, we can assess their individual impact. The compromise of task accuracy (F1) serves as an indicator of the relative importance of the isolated attribute group.

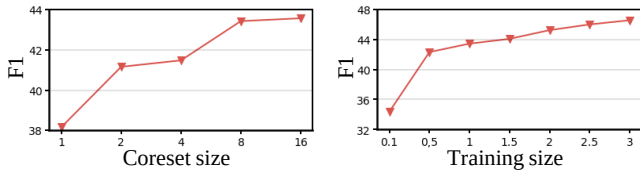


Figure 8: The parameter study of the coreset size (Left) and training size (Right). It exhibits the task accuracy trend with the increment of the indicated parameter.

ings underscore the substantial advancements achieved via joint training in comparison to employing solely rendered data for training purposes. Notably, upon amalgamating the DT set with pseudo-labeled authentic data, a notable 2.21% enhancement in F1 score is observed, signifying the pronounced efficacy of this joint approach over the exclusive use of the DT set.

The superiority of coordinate descent over existing digital twin creation methods. In Fig. 6, the risk curve spans 150 iterations, illustrating convergence patterns of optimization methods, including soft rasterizer, InfoGAN, LDM-based, and coordinate descent. Notably, coordinate descent exhibits a stable convergence, which is a distinctive step-like descent, in contrast to gradient-based behaviors which are usually not stable. This distinction stems from coordinate descent’s search strategy. These observations align with our previous assessment in Table 2. Coordinate descent consistently outperforms others, in terms of both domain gap and the final ARC accuracy.

The superiority of FPS over random sampling. Coreset selection in digital twin creation is crucial, capturing representative images from a large target image pool, thereby reducing the number needed for creating digital twins. To validate the effectiveness of our coreset selection method FPS, we compare it to random selection. In the latter, an equivalent number of images are randomly chosen from the target set. Results in Table 3 highlight FPS’s clear superiority. It exhibits higher task accuracy and domain gap, outperforming random selection by 1.3% and 4.93, respectively.

The superiority of LPIPS. In our experiment, we utilize LPIPS as our loss function for digital twin creation. To gain deeper insights, we explore alternative losses: SSIM (Wang et al. 2004), and StyleLoss (Johnson, Alahi, and Fei-Fei 2016). Results in Table 4 show LPIPS as the superior choice for domain dissimilarity and task accuracy.

Impact of different attributes. In our film scene, we group the attribute vector into three categories, the camera (distance, height), orientation (in-plane rotation, azimuth), and light (intensity). The ablation of each attribute can reveal their impact on task accuracy. In Fig. 7, notably, we observe camera location (distance, height) holds a dominant role in domain dissimilarity. Distant objects exist in object-centric tasks, leading to lower resolution and quality. Lighting and orientation exert similar influences, with a slight orientation advantage due to viewpoint distribution bias.

Parameter study. By default, we select 8 target images per product. Thus the size of D_S^* , $O = 8 \times 116$. Increasing coreset size O enhances target distribution representation but escalates attribute optimization time. Our experi-

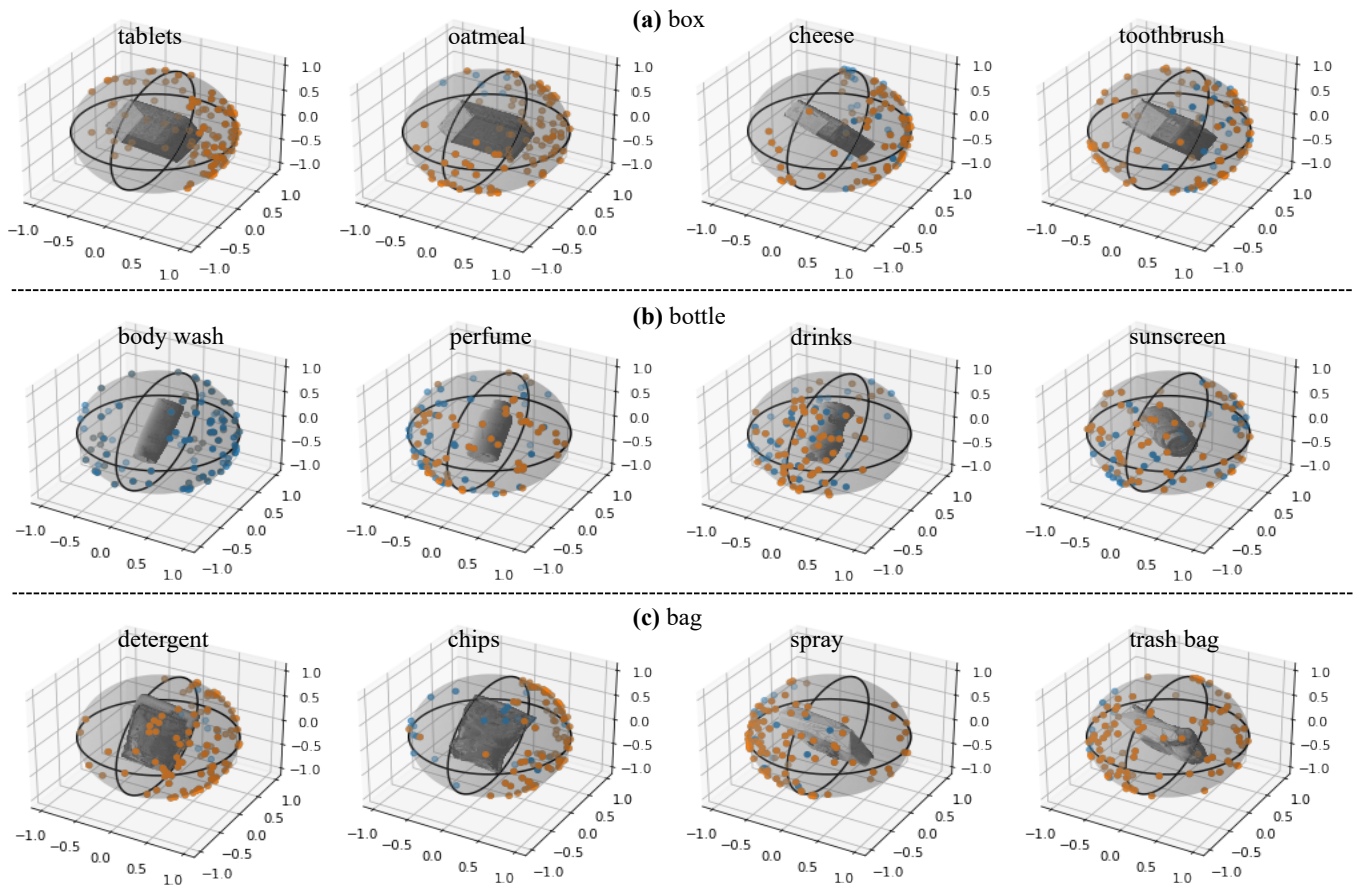


Figure 9: Viewpoint distribution visualization for box, bottle, and bag retail products. Viewpoint distributions are learned by DtTrain. We select 4 products per class, where blue samples imply the in-plane rotation under 30° and orange for above. Each sample, represented by a point surrounding the object, corresponds to learned attributes by DtTrain. Remarkably, the distribution exhibits a non-uniform pattern, resulting in noticeable biases within each class. Our proposed method aims to model the intricate attribute patterns to accurately simulate the biases such that the domain gap is minimized.

ment, depicted in the left of Fig. 8, reveals an evident trend, *i.e.*, larger coreset sizes enhance task accuracy. However, larger coreset sizes also increase the time needed for building a training set. This highlights a trade-off, emphasizing the need to balance accuracy near saturation while maintaining operational efficiency when selecting an optimal coreset size. We observe that beyond a coreset size of 8, accuracy improvement plateaus. Thus by default, 8 target images per product are selected.

In the experiment, we have defaulted the size of a training set N equals 22,000. We also test different training set sizes relative to the default size. Results, shown on the right of Fig. 8, clearly indicate increasing training size enhances task accuracy. However, accuracy improvement plateaus when it reaches the default training set size.

Numerically understanding real ARC bias. The distribution of viewpoints is illustrated in Fig. 9, providing valuable insights into inherent biases. By establishing a correlation between viewpoint distribution bias and the underlying shape characteristics, we can intuitively elucidate the rationale behind these patterns. For instance, the unimodal distri-

bution observed in box-like tablet products indicates a customer preference for holding the product from a specific angle. In comparison, the nearly uniform distribution of body wash can be attributed to the cylindrical symmetry of its bottle-like shape. A bimodal distribution emerges for bag-like objects such as chips, showing customers' viewpoints concentrated at the front and back of the bag.

Conclusion

In conclusion, the automation of the checkout process in smart retail environments has garnered significant attention. However, the scarcity of annotated training data has posed a challenge. To overcome this limitation, we introduced a novel approach utilizing product 3D models for data generation through graphic engine rendering. This approach, termed as DtTrain, can automatically edit the rendered image content in a graphic engine to generate training data with a good resemblance to the real ARC scenario. In addition, using viewpoint as an example, we show that models enable understanding of the dataset (user) bias computing the attribute distribution of given product categories. This article

demonstrates the benefit of training data optimization, and establishes a promising pathway for advancing automated checkout systems in smart retail through robust and representative training data.

Acknowledgement

This work is partially done when Yue has an internship at NVIDIA, with the support of NVIDIA computing resources. This work was also supported in part by the ARC Discovery Project (DP210102801), Oracle Cloud credits, and related resources provided by Oracle for Research.

A Related Works

AutoRetail checkout has been advanced through multimodality, initially relying on barcodes (Sriram et al. 1996), a technology that remains widely used and popular today. Recent developments in deep learning have sparked a shift in ARC research, with a growing emphasis on computer vision approaches. Notably, researchers have explored the utilization of VGG-16 and Inception V3 layers as feature descriptors for image classification of various products (Geng et al. 2018; Chong, Bustan, and Wee 2016). Additionally, deep learning pipelines based on state-of-the-art object detectors have been proposed for product recognition (Tonioni, Serra, and Di Stefano 2018). In contrast, our focus diverges from previous work that primarily emphasized model design and tuning. Instead, we concentrate on rendered image creation and optimization, aligning with the downstream task and target domain.

Training with rendered data. Data rendering via graphic engine has emerged as a cost-effective alternative to real labeled data, which can often be expensive to obtain. Various studies have explored the integration of rendered data alongside real data in the training set to improve model accuracy (Yao et al. 2020; Zheng, Zheng, and Yang 2017). Additionally, some researchers have delved into training models exclusively on rendered data (Kar et al. 2019). In the context of this paper, we concentrate on leveraging rendered data exclusively to develop automatic retail systems.

Existing training set optimization methods. Leveraging rendered data offers the advantages of increased label availability and enhanced flexibility in the training process. However, it also introduces challenges, most notably the domain gap that exists between the source and target domains, thereby reducing task accuracy. Many existing studies employ reinforcement learning (RL) to improve task accuracy by optimizing rendering attributes (Kar et al. 2019; Devaranjan, Kar, and Fidler 2020; Ruiz, Schuler, and Chandraker 2019; Xue, Mao, and Zheng 2021). For instance, Kar *et al.* use policy gradients to optimize scene layout. In comparison, Yao *et al.* formulate attribute optimization as a search problem due to challenges in obtaining attribute gradients, proposing a pruned greedy search called attribute descent (Yao et al. 2020). However, these existing methods still require the manual definition of attribute distributions, which involves significant human effort. In this paper, we introduce the DtTrain framework, which minimizes the need for human-designed attribute distributions while achieving

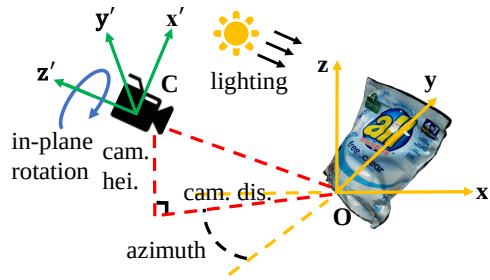


Figure 10: Controllable attributes defined in our film scene. Inherited from the film scene proposed by Yao et al. (2022), we have the attributes that include in-plane rotation, azimuth, camera distance, camera height and lighting.

higher task accuracy. With DtTrain, the burden of distribution design is reduced, providing a more efficient and effective approach to attribute optimization.

B Film Scene

We consider that the content disparity in images arises from various prime factors. In this context, a rendered image is created through a renderer, which is conditioned on attributes including azimuth, in-plane rotation, lighting intensity, lighting angle, camera distance, and height. These attributes are defined in the work by Yao et al. (2022) and are explained in Fig. 10. This supplementary figure complements the information presented in Fig. 1, providing a more detailed understanding of the physical significance of these attributes.

We first constrain the rotation attributes, namely in-plane rotation, azimuth, and light direction, to fall within the range of 0° to 360° . Subsequently, the light intensity is deliberately designed to vary between 0 and 100. Here, a value of 0 signifies complete darkness, while a value of 100 corresponds to full illumination. Regarding camera height and distance, we refrain from explicitly specifying a range limit, varying between 0 and 100. Since we use coordinate descent, a search-based technique for obtaining digital twins. To accommodate this, we define search spaces $S = [S_1, \dots, S_K]$ for each attribute in the attribute list $\psi = [\psi_1, \dots, \psi_K]$. For example, we define the search space of rotation attributes, which lies in the range of 0° to 360° that has 30° degrees intervals. For the search space of camera height and camera distance, we have a range of 0 to 100 that has 10 intervals. In the context of coordinate descent, a balance between interval size and search space emerges, *i.e.*, small intervals correspond to expansive search spaces, while larger intervals narrow down exploration. To ensure experimental fairness, we maintain a consistency akin to Yao et al. (2022).

C Existing Optimization Methods

We compare our methods with various existing optimization strategies from previous research in the experiment. As mentioned in our experiment part, we compare DtTrain with existing training set optimization methods, and we compare

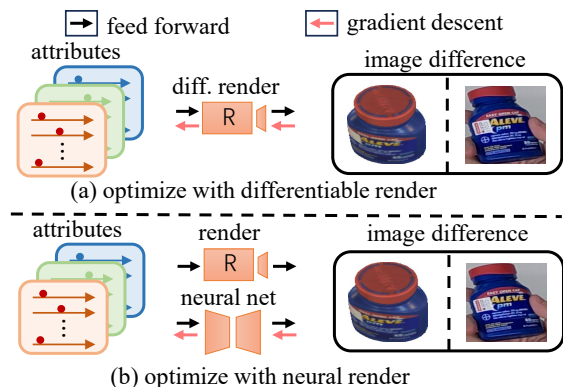


Figure 11: Existing two methods for creating digital twins, differentiable rendering and neural rendering. For the differentiable renderer, the gradient can directly backpropagate through the renderer to optimize the attributes. For the neural renderer, we create a conditional neural network to emulate differentiable renderers.

coordinate descent with existing digital twin creation methods.

Existing Training Set Optimization Methods

We utilize two well-established techniques frequently employed for creating training datasets using the graphical engine. These techniques are known as LTS (Ruiz, Schultze, and Chandraker 2019) and attribute descent (Yao et al. 2022). These approaches belong to the realm of attribute distribution optimization, as they require the initial specification of attribute distributions followed by subsequent optimization of parameters.

Learning to Simulate (LTS) (Ruiz, Schultze, and Chandraker 2019) is a typical distribution-based reinforcement learning approach, where the controllable attributes are optimized by maximizing the reward accumulated in the downstream task. Despite the simple design, the end-to-end learning architecture implies it is difficult to combine with complicated downstream tasks. In our experiment, we regard it as an ad-hoc benchmark in conventional distribution optimization approaches.

Attribute descent (Yao et al. 2022) is a gradient-free search strategy to get an optimized training set. During the search stage, it can significantly reduce the search space of the distribution parameters. Furthermore, attribute descent is guaranteed to find the sub-optimal solutions by iterating a single element while keeping others frozen.

Existing Digital Twin Creation Methods

For both differentiable rendering and neural rendering, we use the same loss as coordinate descent, LPIPS.

Differentiable rendering refers to a renderer that preserves gradients in the rendering function, shown in Fig. 11 top. In our experiment, we use a differentiable renderer called soft rasterizer (Liu et al. 2019), which is implemented in Pytorch3D (Ravi et al. 2020). In the soft rasterizer, the gradient can directly backpropagate through the renderer,

thereby enabling the editing of attributes to create digital twins.

Neural rendering can be seen as a similar form of differentiable renderer as it also enables gradient-based optimization. This approach performs backpropagation through the neural network, which serves as an imitator of a non-differentiable renderer. This approach is originally proposed by (Shi et al. 2019) to create digital twins for face images. Motivated by their methods, we have an adapted version to create digital twins for product images. Specifically, as shown in Fig. 11 bottom. The whole process involves two stages. In the first stage, we train the conditional generative neural network using the attributes and their corresponding rendered images. In the second stage, we freeze the network while backpropagating gradients through the neural renderer, thereby enabling the editing of attributes to create digital twins.

In the experiment, we utilize two typical conditional generative networks: InfoGAN (Chen et al. 2016) and latent diffusion model (LDM) (Rombach et al. 2022). By modifying specific tailored latent variables, the InfoGAN can generate product images with desired attributes. Likewise, LDM is widely popular due to its strong representation capabilities and high-quality outputs. In our experiment, we adopt the pre-trained stable diffusion model from (Rombach et al. 2022) and fine-tune it on our created retail training set. As the original architecture only supports text prompts, we make adjustments by removing the CLIP encoder (Radford et al. 2021), and replacing it with a lightweight, zero-initialized attribute encoder. For LDM training, we train the entire U-Net (Ronneberger, Fischer, and Brox 2015) along with the attribute encoder to adapt the model to our retail products.

As shown in our experimental results, we demonstrate that coordinate descent consistently outperforms both differentiable rendering and neural rendering. While both differentiable rendering and neural rendering involve the iterative update of attributes through gradient descent. It is noteworthy that, in contrast to coordinate descent, these gradient descent-based approaches are susceptible to becoming entrapped within local minima. To illustrate, consider a nearly symmetrical retail product, such as a box-shaped item, where viewpoint local minima exist both on the product’s front and rear sides. Despite the global minimum residing exclusively on the product’s front side, gradient descent-based methods can easily become “trapped” in the local minimum of the rear side. In comparison, coordinate descent exhibits the ability to escape such entrapment due to its inherent search-based nature.

D Task Model

We provide a comprehensive overview of the task model employed in our experiment for evaluating rendered retail data. The ARC pipeline, as encapsulated by Naphade et al. (2022), unfolds as three distinct stages: detection, tracking, and counting (DTC).

Initiating with the detection stage, our objective revolves around the identification and classification of target products within video content. To this end, we harness the power

of YOLOv5 (Jocher et al. 2022), which is pertained on COCO (Lin et al. 2014) and further fine-tuned using our rendered data. The outcome manifests as estimated bounding boxes, and the classification process culminates in an ensemble of three models: Res2Net (Gao et al. 2019), Swin-Transformer (Liu et al. 2021), and RepVGG (Ding et al. 2021).

Transitioning seamlessly to the tracking stage, our focal point lies in establishing continuity in tracking identical products across diverse frames. This mitigates the risk of count duplication. We use the tracking algorithm, *i.e.*, ByteTrack (Zhang et al. 2022), which aptly achieves track matching and effectively circumvents the challenge posed by object occlusion. Finally, in the counting stage, the goal is to predict each product uniquely, avoiding any redundancy. To this end, trajectory counting is employed, with each trajectory being assigned a time prediction rooted in the highest level of confidence.

References

- Chen, X.; Duan, Y.; Houthoofd, R.; Schulman, J.; Sutskever, I.; and Abbeel, P. 2016. Infogan: Interpretable representation learning by information maximizing generative adversarial nets. *Advances in neural information processing systems*, 29.
- Chong, T.; Bustan, I.; and Wee, M. 2016. Deep learning approach to planogram compliance in retail stores. *Semantic Scholar*, 1–6.
- Corbiere, C.; Ben-Younes, H.; Ramé, A.; and Ollion, C. 2017. Leveraging weakly annotated data for fashion image retrieval and label prediction. In *Proceedings of the IEEE international conference on computer vision workshops*, 2268–2274.
- Devaranjan, J.; Kar, A.; and Fidler, S. 2020. Meta-sim2: Unsupervised learning of scene structure for synthetic data generation. In *European Conference on Computer Vision*, 715–733. Springer.
- Ding, X.; Zhang, X.; Ma, N.; Han, J.; Ding, G.; and Sun, J. 2021. Repvgg: Making vgg-style convnets great again. In *Proceedings of the IEEE/CVF conference on computer vision and pattern recognition*, 13733–13742.
- Dong, X.; Zhan, X.; Wu, Y.; Wei, Y.; Kampffmeyer, M. C.; Wei, X.; Lu, M.; Wang, Y.; and Liang, X. 2022. M5product: Self-harmonized contrastive learning for e-commercial multi-modal pretraining. In *Proceedings of the IEEE/CVF Conference on Computer Vision and Pattern Recognition*, 21252–21262.
- Eldar, Y.; Lindenbaum, M.; Porat, M.; and Zeevi, Y. Y. 1997. The farthest point strategy for progressive image sampling. *IEEE Transactions on Image Processing*, 6(9): 1305–1315.
- Farahani, R. Z.; and Hekmatfar, M. 2009. *Facility location: concepts, models, algorithms and case studies*. Springer Science & Business Media.
- Gao, S.-H.; Cheng, M.-M.; Zhao, K.; Zhang, X.-Y.; Yang, M.-H.; and Torr, P. 2019. Res2net: A new multi-scale backbone architecture. *IEEE transactions on pattern analysis and machine intelligence*, 43(2): 652–662.
- Geng, W.; Han, F.; Lin, J.; Zhu, L.; Bai, J.; Wang, S.; He, L.; Xiao, Q.; and Lai, Z. 2018. Fine-grained grocery product recognition by one-shot learning. In *Proceedings of the 26th ACM international conference on Multimedia*, 1706–1714.
- Heusel, M.; Ramsauer, H.; Unterthiner, T.; Nessler, B.; and Hochreiter, S. 2017. Gans trained by a two time-scale update rule converge to a local nash equilibrium. In *Advances in neural information processing systems*.
- Jocher, G.; Chaurasia, A.; Stoken, A.; Borovec, J.; NanoCode012; Kwon, Y.; Michael, K.; TaoXie; Fang, J.; imyhxy; Lorna; Yifu, Z.; Wong, C.; V, A.; Montes, D.; Wang, Z.; Fati, C.; Nadar, J.; Laughing; UnglvKitDe; Sonck, V.; tkianai; yxNONG; Skalski, P.; Hogan, A.; Nair, D.; Strobel, M.; and Jain, M. 2022. ultralytics/yolov5: v7.0 - YOLOv5 SOTA Realtime Instance Segmentation.
- Johnson, J.; Alahi, A.; and Fei-Fei, L. 2016. Perceptual losses for real-time style transfer and super-resolution. In *Computer Vision—ECCV 2016: 14th European Conference, Amsterdam, The Netherlands, October 11–14, 2016, Proceedings, Part II 14*, 694–711. Springer.
- Kar, A.; Prakash, A.; Liu, M.-Y.; Cameracci, E.; Yuan, J.; Rusiniak, M.; Acuna, D.; Torralba, A.; and Fidler, S. 2019. Meta-Sim: Learning to Generate Synthetic Datasets. In *Proceedings of the IEEE International Conference on Computer Vision*.
- Lin, T.-Y.; Maire, M.; Belongie, S.; Hays, J.; Perona, P.; Ramanan, D.; Dollár, P.; and Zitnick, C. L. 2014. Microsoft coco: Common objects in context. In *European conference on computer vision*, 740–755. Springer.
- Liu, F.; Chen, D.; Du, X.; Gao, R.; and Xu, F. 2023. MEP-3M: A large-scale multi-modal E-commerce product dataset. *Pattern Recognition*, 140: 109519.
- Liu, S.; Li, T.; Chen, W.; and Li, H. 2019. Soft rasterizer: A differentiable renderer for image-based 3d reasoning. In *Proceedings of the IEEE/CVF International Conference on Computer Vision*, 7708–7717.
- Liu, Z.; Lin, Y.; Cao, Y.; Hu, H.; Wei, Y.; Zhang, Z.; Lin, S.; and Guo, B. 2021. Swin transformer: Hierarchical vision transformer using shifted windows. In *Proceedings of the IEEE/CVF international conference on computer vision*, 10012–10022.
- Naphade, M.; Wang, S.; Anastasiu, D. C.; Tang, Z.; Chang, M.-C.; Yao, Y.; Zheng, L.; Rahman, M. S.; Venkatachalapathy, A.; Sharma, A.; Feng, Q.; Ablavsky, V.; Sclaroff, S.; Chakraborty, P.; Li, A.; Li, S.; and Chellappa, R. 2022. The 6th AI City Challenge. arXiv:2204.10380.
- Nguyen, T. C.; Phan, N. L.; and Nguyen, S. T. 2022. Improving Domain Generalization by Learning without Forgetting: Application in Retail Checkout. *arXiv preprint arXiv:2207.05422*.
- Radford, A.; Kim, J. W.; Hallacy, C.; Ramesh, A.; Goh, G.; Agarwal, S.; Sastry, G.; Askell, A.; Mishkin, P.; Clark, J.; et al. 2021. Learning transferable visual models from natural language supervision. In *International conference on machine learning*, 8748–8763. PMLR.

- Ravi, N.; Reizenstein, J.; Novotny, D.; Gordon, T.; Lo, W.-Y.; Johnson, J.; and Gkioxari, G. 2020. Accelerating 3D Deep Learning with PyTorch3D. *arXiv:2007.08501*.
- Richter, S. R.; Vineet, V.; Roth, S.; and Koltun, V. 2016. Playing for data: Ground truth from computer games. In *European Conference on Computer Vision*.
- Ristani, E.; Solera, F.; Zou, R.; Cucchiara, R.; and Tomasi, C. 2016. Performance Measures and a Data Set for Multi-Target, Multi-Camera Tracking. In *European Conference on Computer Vision workshop on Benchmarking Multi-Target Tracking*.
- Rombach, R.; Blattmann, A.; Lorenz, D.; Esser, P.; and Ommer, B. 2022. High-resolution image synthesis with latent diffusion models. In *Proceedings of the IEEE/CVF Conference on Computer Vision and Pattern Recognition*, 10684–10695.
- Ronneberger, O.; Fischer, P.; and Brox, T. 2015. U-net: Convolutional networks for biomedical image segmentation. In *International Conference on Medical image computing and computer-assisted intervention*, 234–241. Springer.
- Ruiz, N.; Schuler, S.; and Chandraker, M. 2019. Learning to simulate. In *Proceedings of the International Conference on Learning Representations*.
- Sakaridis, C.; Dai, D.; and Van Gool, L. 2018. Semantic foggy scene understanding with synthetic data. *International Journal of Computer Vision*, 1–20.
- Sener, O.; and Savarese, S. 2018. Active Learning for Convolutional Neural Networks: A Core-Set Approach. In *International Conference on Learning Representations*.
- Shi, T.; Yuan, Y.; Fan, C.; Zou, Z.; Shi, Z.; and Liu, Y. 2019. Face-to-parameter translation for game character auto-creation. In *Proceedings of the IEEE/CVF International Conference on Computer Vision*, 161–170.
- Sriram, T.; Rao, K. V.; Biswas, S.; and Ahmed, B. 1996. Applications of barcode technology in automated storage and retrieval systems. In *Proceedings of the 1996 IEEE IECON. 22nd International Conference on Industrial Electronics, Control, and Instrumentation*, volume 1, 641–646. IEEE.
- Sun, X.; and Zheng, L. 2019. Dissecting Person Re-identification from the Viewpoint of Viewpoint. In *Proceedings of the IEEE/CVF Conference on Computer Vision and Pattern Recognition*.
- Tonioni, A.; Serra, E.; and Di Stefano, L. 2018. A deep learning pipeline for product recognition on store shelves. In *2018 IEEE International Conference on Image Processing, Applications and Systems (IPAS)*, 25–31. IEEE.
- Tremblay, J.; Prakash, A.; Acuna, D.; Brophy, M.; Jampani, V.; Anil, C.; To, T.; Cameracci, E.; Boochoon, S.; and Birchfield, S. 2018. Training deep networks with synthetic data: Bridging the reality gap by domain randomization. In *Proceedings of the IEEE/CVF Conference on Computer Vision and Pattern Recognition Workshops*.
- Wang, Z.; Bovik, A. C.; Sheikh, H. R.; and Simoncelli, E. P. 2004. Image quality assessment: from error visibility to structural similarity. *IEEE transactions on image processing*, 13(4): 600–612.
- Wei, X.-S.; Cui, Q.; Yang, L.; Wang, P.; and Liu, L. 2019. RPC: A large-scale retail product checkout dataset. *arXiv preprint arXiv:1901.07249*.
- Williamson, D. P.; and Shmoys, D. B. 2011. *The design of approximation algorithms*. Cambridge university press.
- Wright, S. J. 2015. Coordinate descent algorithms. *Mathematical Programming*, 151(1): 3–34.
- Xue, Z.; Mao, W.; and Zheng, L. 2021. Learning to Simulate Complex Scenes for Street Scene Segmentation. *IEEE Transactions on Multimedia*.
- Yao, Y.; Zheng, L.; Yang, X.; Naphade, M.; and Gedeon, T. 2020. Simulating Content Consistent Vehicle Datasets with Attribute Descent. In *Proceedings of the European Conference on Computer Vision*.
- Yao, Y.; Zheng, L.; Yang, X.; Naphade, M.; and Gedeon, T. 2022. Attribute Descent: Simulating Object-Centric Datasets on the Content Level and Beyond. *arXiv preprint arXiv:2202.14034*.
- Zhan, X.; Wu, Y.; Dong, X.; Wei, Y.; Lu, M.; Zhang, Y.; Xu, H.; and Liang, X. 2021. Product1m: Towards weakly supervised instance-level product retrieval via cross-modal pretraining. In *Proceedings of the IEEE/CVF International Conference on Computer Vision*, 11782–11791.
- Zhang, R.; Isola, P.; Efros, A. A.; Shechtman, E.; and Wang, O. 2018. The unreasonable effectiveness of deep features as a perceptual metric. In *Proceedings of the IEEE conference on computer vision and pattern recognition*, 586–595.
- Zhang, Y.; Sun, P.; Jiang, Y.; Yu, D.; Weng, F.; Yuan, Z.; Luo, P.; Liu, W.; and Wang, X. 2022. Bytetrack: Multi-object tracking by associating every detection box. In *European Conference on Computer Vision*, 1–21. Springer.
- Zheng, Z.; Zheng, L.; and Yang, Y. 2017. Unlabeled samples generated by gan improve the person re-identification baseline in vitro. In *Proceedings of the IEEE/CVF Conference on Computer Vision and Pattern Recognition*, 3754–3762.